International Conference on Textile Composites and Inflatable Structures
STRUCTURAL MEMBRANES 2011
E. Oñate, B. Kröplin and K.-U.Bletzinger (Eds)

DIRECT AREA MINIMIZATION THROUGH DYNAMIC RELAXATION

RUY M. O. PAULETTI[*], **DANIEL M. GUIRARDI**[†]

[*]Polytechnic School of the University of São Paulo
P.O. Box 61548, 05424-970 São Paulo, Brazil
e-mail: pauletti@usp.br, web Page: WWW.lmc.ep.usp.br/people/pauletti

Key words: area minimization, dynamic relaxation method, membrane structures, nonlinear analysis

Summary. Minimal surfaces, characterized by the property of a minimal area within a fixed boundary, offer an interesting design option for membrane structures, since they are uniquely defined and provide economy of material and more regular fabric patterns. Analytical solution for the non-linear equation governing area minimization may be rather difficult for complex boundaries, leaving numerical solution as the only general way to tackle with the problem. In this paper we show that the dynamic relaxation method offers an interesting alternative to solve the area minimization problem, first interpreted as a nonlinear equilibrium problem, then replaced by a pseudo-dynamic analysis, where fictitious masses and damping matrices are arbitrarily chosen to control the stability of the time integration process.

1 INTRODUCTION

The study of minimal surfaces is important both from theoretical and practical points of view. Minimal surfaces are characterized by the property of a minimal area within a fixed boundary. They are also the solution geometry for a membrane constringed to that same boundary, and under an isotropic and uniform plane stress field[1,2,3]. These properties render minimal surfaces an interesting design option for membrane structures, since they are uniquely defined, for a given boundary, and provide economy of material and more regular fabric patterns[4,5,6,7,8].

Minimal surfaces have also attracted the interest of scientists since the times of Lagrange (who solved the problem for some surfaces of the type $z = f(x, y)$) and Euler (who proved that minimal surfaces have zero-mean curvature everywhere, and therefore are either plane or anticlastic). Euler was also the first to find the *catenoid* (the minimum surface bounded by two parallel, co-axial rings), which remains one of the few analytical solutions available to this class of problems. In the nineteenth century, the Belgian physicist Joseph Plateau showed that analogue solutions to area minimization problems could be produced by dipping wire frameworks into a bath of soap solution.

2 AREA MINIMIZATION WITH FIXED BOUNDARIES

For the moment, we restrain ourselves to surfaces bounded by closed curves C embedded into Euclidian tridimensional space R^3 and spanned by a vector field $\boldsymbol{x} = \boldsymbol{x}(\theta_1, \theta_2)$, where θ_1 and θ_2 are continuous and monotonous parameters, as sketched in Figure 1.

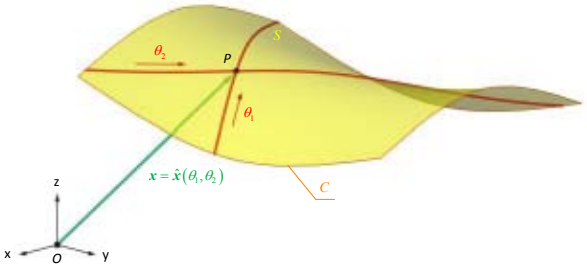

Figure 1: A tridimensional surface bounded by a closed curve C and spanned by a vector field $\boldsymbol{x} = \boldsymbol{x}(\theta_1, \theta_2)$ (adapted from reference [8])

At every point $P \in S$, we define vectors $\boldsymbol{g}_\alpha = \dfrac{\partial \boldsymbol{x}}{\partial \theta_\alpha}$, $\alpha = 1, 2$, tangent to the surface. A unit vector, normal to the surface S at P, is given by $\boldsymbol{g}_3 = \boldsymbol{g}_1 \times \boldsymbol{g}_2 / \|\boldsymbol{g}_1 \times \boldsymbol{g}_2\|$. The total area of any such a surface is given by

$$A = \int_S dA = \int_S \|\boldsymbol{g}_1 \times \boldsymbol{g}_2\| \, d\theta_1 \, d\theta_2 \tag{1}$$

We seek a surface S^*, spanned by a vector field $\boldsymbol{x}^*$, such that its area A^* is a minimum. In other words, for any perturbation field $\delta \boldsymbol{u}$ around $\boldsymbol{x}^*$, compatible with C, there must hold

$$\delta A^* = \left.\frac{\partial A}{\partial \boldsymbol{x}}\right|_{\boldsymbol{x}^*} \delta \boldsymbol{u} = 0, \quad \forall \delta \boldsymbol{u} . \tag{2}$$

Thus, the necessary 1st order condition for a configuration $\boldsymbol{x}^*$ to be minimal is given by the non-linear equation

$$\left.\frac{\partial A}{\partial \boldsymbol{x}}\right|_{\boldsymbol{x}^*} = 0 , \tag{3}$$

with the equality restriction $(\boldsymbol{x}_P - \bar{\boldsymbol{x}}_P) = \boldsymbol{0}, \forall P \in C$, where $\bar{\boldsymbol{x}}_P$ is a vector function spanning the prescribed coordinates at $P \in C$.

The field of global coordinates $\boldsymbol{x}$ spanning a generic configuration S can also be decomposed according to $\boldsymbol{x} = \boldsymbol{x}^r + \boldsymbol{u}$, where $\boldsymbol{x}^r$ spans an initial given configuration and $\boldsymbol{u}$ is a displacement vector field. Now, since $\boldsymbol{x}^r$ is constant, and derivatives can be taken indistinctly with respect to global coordinates $\boldsymbol{x}$ or to displacements $\boldsymbol{u}$, the solution to the area minimization problem consists in finding the configuration $\boldsymbol{u}^*$ such that

$$\boldsymbol{p}(\boldsymbol{u}^*) = \left.\frac{\partial A}{\partial \boldsymbol{u}}\right|_{\boldsymbol{u}^*} = \boldsymbol{0} , \tag{4}$$

where we define the *generalized internal load vector* $\boldsymbol{p}(\boldsymbol{u}) = \left|\frac{\partial A}{\partial \boldsymbol{u}}\right|$.

Analytical solution of the nonlinear Eq. (3) or Eq. (4) may be rather difficult for complex boundary geometries, leaving numerical solution as the only general way to tackle with the problem.

2.1 Discretization

In order to numerically solve Eq. (4), it is necessary to replace the continuous fields $\boldsymbol{x}^r$, $\boldsymbol{u}$ and $\boldsymbol{p}$ by some convenient algebraic approximation. Faceted surfaces, although not globally differentiable, offer a convenient alternative for the numerical estimative of the total area of smooth surfaces, improving numerical precision as the number of facets is increased. In this paper, we choose to work with flat triangular facets (the simplest possible choice), laid onto a mesh of n nodes, whose coordinates are collected in a *global position vector* $\mathbf{x} = \begin{bmatrix} \mathbf{x}_1^T & \mathbf{x}_2^T & \dots & \mathbf{x}_n^T \end{bmatrix}^T$, where $\mathbf{x}_i = [\boldsymbol{x}_i]$ stores the Cartesian coordinates of the i^{th} node of the mesh. Nodal displacement can also be grouped in a *global displacement vector* $\mathbf{u} = \begin{bmatrix} \mathbf{u}_1^T & \mathbf{u}_2^T & \dots & \mathbf{u}_n^T \end{bmatrix}^T_{3n\times 1}$, where $\mathbf{u}_i = [\boldsymbol{u}_i]$ stores the Cartesian components of the displacement of the i^{th} node. Note the double transpositions present in these definitions, used simply to avoid a column-wise notation.

Figure 2 shows the basic geometric quantities required for the definition of a generic triangular facet (an 'element') of index e. Facet nodes and edges are numbered with edges facing nodes of same number. We extract the element nodal coordinates and displacements from the global position and displacement vectors according to $\mathbf{x}^e = \mathbf{C}^e\mathbf{x}$, and $\mathbf{u}^e = \mathbf{C}^e\mathbf{u}$, where $\mathbf{C}^e$ is the order $9\times 3n$ Boolean incidence matrix of that element, which correlates the local node numbers $\{1,2,3\}$ with the global numbers $\{i,j,k\}$ such that $\mathbf{C}^e_{1i} = \mathbf{C}^e_{2j} = \mathbf{C}^e_{3j} = \mathbf{I}_3$ and $\mathbf{C}^e_{1m} = \mathbf{C}^e_{2m} = \mathbf{C}^e_{3m} = \mathbf{0}$, $m \notin \{i,j,k\}$, where $\mathbf{0}$ and $\mathbf{I}_3$ are, respectively, the null and identity matrices of order three. Of course, these definitions are merely formal, and computer implementation avoids the multiplicity of zero multiplications they contain.

The lengths of the edges of a generic triangular facet can then be computed by $\ell^e_i = \left\|\mathbf{l}^e_i\right\| = \left\|\mathbf{x}^e_k - \mathbf{x}^e_j\right\|$, with indexes $i,j,k = 1,2,3$ in cyclic permutation. Unit vectors parallel to the element edges are denoted by $\mathbf{v}^e_i = \mathbf{l}^e_i / \left\|\mathbf{l}_i\right\|$. Now, an element area vector is defined as $\mathbf{a}^e = \frac{1}{2}\left(\mathbf{l}^e_1 \times \mathbf{l}^e_2\right)$, and the element scalar area is given by $A^e = \left\|\mathbf{a}^e\right\|$, whilst $\mathbf{n}^e = \mathbf{a}^e / A^e$ is an unit vector, normal to the plane of the facet. A coherent node numbering for all the elements provides an oriented surface.

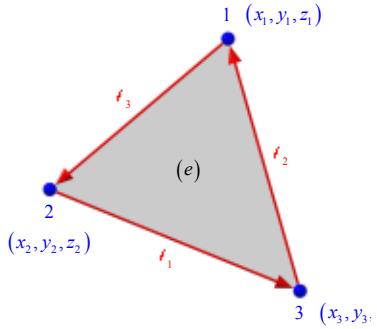

Figure 2: A triangular facet.

The total area of a smooth surface discretized by a mesh of n_e triangular facets is then, approximately,

$$A = \sum_{e=1}^{n_e} A^e = \sum_{e=1}^{n_e} \tfrac{1}{2} \left\| \left(\mathbf{l}_1^e \times \mathbf{l}_2^e \right) \right\| \tag{5}$$

2.2 Newton's Method

Although in this paper we are concerned with solving the area minimization via dynamic relaxation, for the sake of comparison we now remind that the more popular method for the numerical solution of nonlinear systems is Newton's Method, in which the solution $\boldsymbol{u}^*$ is sought starting from an initial estimative $\boldsymbol{u}_0$ and iterating the recurrence formula

$$\boldsymbol{u}_{i+1} = \boldsymbol{u}_i - \boldsymbol{H}_i^{-1} \boldsymbol{p}_i , \tag{6}$$

where we define the *Hessian tensor,* $\boldsymbol{H} = \dfrac{\partial \boldsymbol{p}}{\partial \boldsymbol{u}} = \dfrac{\partial^2 A}{\partial \boldsymbol{u}^2}$.

Now, introducing in (6) the area approximation (5), we obtain an *approximate generalized internal load* vector as

$$\boldsymbol{p} = \sum_{e=1}^{n_e} \mathbf{C}^{eT} \mathbf{p}^e \tag{7}$$

where we define the *element internal load vector,* $\mathbf{p}^e = \dfrac{\partial A^e}{\partial \mathbf{u}^e}$.

By its turn, the Hessian tensor is approximated by

$$\boldsymbol{H} \approx \sum_{e=1}^{ne} \mathbf{C}^{eT} \mathbf{H}^e \mathbf{C}^e , \tag{8}$$

where we define the *element Hessian matrix,* $\mathbf{H}^e = \dfrac{\partial \mathbf{p}^e}{\partial \mathbf{u}^e}$.

Deriving the area of a facet with respect to its displacements $\mathbf{u}^e$, after some algebra, there results for the element internal load vector:

$$\mathbf{p}^e = -\frac{1}{2} \boldsymbol{\Lambda}^e \mathbf{n}^e \tag{9}$$

where $\mathbf{\Lambda}^e = \begin{bmatrix} \mathbf{\Lambda}_1^{eT} & \mathbf{\Lambda}_2^{eT} & \mathbf{\Lambda}_3^{eT} \end{bmatrix}^T$, with $\mathbf{\Lambda}_k^e = skew\left(\mathbf{l}_k^e\right)$.

Again deriving (9) with respect to displacements $\mathbf{u}^e$, one gets the element Hessian matrix:

$$\mathbf{H}^e = \frac{1}{4A^e}\left(\mathbf{\Lambda}^e\mathbf{\Gamma}^e\mathbf{\Lambda}^{eT} + 2\mathbf{\Psi}^e\right) \tag{10}$$

where $\mathbf{\Gamma}^e = \mathbf{I}_3 - \mathbf{n}^e\mathbf{n}^{e^T}$ and $\mathbf{\Psi}^e = skew(\mathbf{\Omega}^e)$, and where $\mathbf{\Omega}^e = skew\left(\boldsymbol{a}^e\right)$. It is seen that $\mathbf{\Psi}^e$ and therefore $\mathbf{H}^e$ are both symmetric matrices.

However, it is intuitive to realize that the area of any smooth surface, of fixed boundary, is indifferent to deformations involving infinitesimal displacements tangent to the surface itself. In the case of a curved surface divided into a finite number of plane triangular facets, this property is not exact, but anyway, for every given mesh topology, there exists generally an infinity of possible nodal configurations, approximating the same smooth surface. This reflects in the fact that the Hessian matrix (8) becomes more and more ill-conditioned, as long as the solution is approached, and as long as the mesh is refined. In practice, this characteristic overrules the direct solution of (4) by means of pure Newton's method.

On the other hand, deformations involving displacement transversal to surface are in general capable to alter its area. Thus a way to circumvent this problem is the imposition that the nodal displacements have always a component transversal to the current configuration. A particular case, where this restriction is naturally inserted is given by surfaces described by functions $z = \hat{z}(x, y)$, which reduce the area minimization problem to a scalar degree of freedom at every node, as studied in reference[7]. In the general tridimensional case, however, even this restriction degrades as a solution is approached.

Because of these restrictions, it is usual in the problem of area minimization to replace Newton's Method by other algorithms that avoid the exact inversion of the Hessian matrix, such as conjugate gradient methods (as done in references[7,8]), or the BFGS algorithm (as done in reference[9]), which are capable to converge to one of the infinite solutions that exist for any given mesh topology.

2.3 The Dynamic Relaxation Method

The dynamic relaxation method (DRM) offers another interesting alternative to solve complicated nonlinear equilibrium problems, replacing the static equilibrium problem by a pseudo-dynamic analysis, where fictitious masses and damping matrices are arbitrarily chosen to control the stability of the time integration process.

Thus, instead of solving (4), we may follow the damped vibrations of the dynamic system

$$\mathbf{M}\ddot{\mathbf{u}} + \mathbf{C}\dot{\mathbf{u}} + \mathbf{p}(\mathbf{u}) = \mathbf{0} \tag{11}$$

until it comes to a rest, at a solution of Eq. (4). Usually, damping coefficients close to the system's critical damping are chosen, in order to speed up the convergence to the static equilibrium configuration.

Although the dynamic relaxation method shows no advantage for small to medium sized problems, whenever Newton's Method shows good convergence, there may be considerable economy for very large problems. The rationale is that, as long as the computational costs for Newton's method grows with the square of the number of degrees of freedom, and the cost of

DRM grows linearly, there must be a particular number above which Newton's costs becomes larger than DRM costs.

However, this idea cannot be plainly taken, since, when discretization of a given structure is refined, a critical time-step which governs the numerical stability of the system is also reduced, and thus more steps are required for the system to rest.

Nevertheless, since in the DRM the mass and damping matrices are fictitious, they may be adjusted to keep the time-increments small enough to guarantee stability, but as large as possible to reduce the number of steps required for convergence to the static solution.

2.4 Kinetic damping

Several strategies have been devised along the years to define proper damping matrix for the DRM, but we choose here to circumvent the problem altogether, adopting the process of *kinetic damping*, first proposed in reference[10], whereby the undamped movement of the system, governed by

$$\mathbf{M}\ddot{\mathbf{u}} + \mathbf{p}(\mathbf{u}) = \mathbf{0}, \tag{12}$$

is followed until a maximum of the total kinetic energy is reached, when all the velocity components are cancelled, keeping the current geometry. The pseudo-dynamic analysis is then restarted until new kinetic energy maxima (usually smaller than the precedent ones) are found, and all velocities are zeroed once again. The process is repeated until all kinetic energy is dissipated, thus reaching the static equilibrium configuration. The transient of the system's kinetic energy provides a visual criterion for convergence.

2.5 Central differences

In-depth discussions on the relative performance of the several finite-difference schemes available to solve Eq. (12) can be found in references[11,12,13,14,15]. Experience has shown that a convenient choice is offered by the ***central difference method***, which yields an explicit time-integration scheme, when the mass matrix is diagonal, rendering very fast the calculation of every time-step.

In this paper we have adopted a particular brand of the central-difference scheme, progressing from time t_k to time t_{k+1} according to

$$\dot{\mathbf{u}}_{k+\frac{1}{2}} = \dot{\mathbf{u}}_{k-\frac{1}{2}} + \Delta t_k \mathbf{M}^{-1}\mathbf{p}_k \tag{13}$$

$$\mathbf{u}_{k+1} = \mathbf{u}_k + \dot{\mathbf{u}}_{k+\frac{1}{2}}\Delta t_{k+\frac{1}{2}}, \tag{14}$$

where $\Delta t_{k+\frac{1}{2}} = \left(\Delta t_k + \Delta t_{k+1}\right)/2$.

Then we update the geometry according to $\mathbf{x}_{k+1} = \mathbf{x}_0 + \mathbf{u}_{k+1}$. Although more memory is required to store both $\mathbf{x}_0$ and $\mathbf{u}_{k+1}$, it has been observed that this scheme is less sensitive to round-off errors.

2.6 Numerical stability

The central difference method is only conditionally stable, and time increments must be kept sufficiently small. It can be shown that for linear multiple degrees of freedom (MDOF) systems, numerical stability is guaranteed by

$$\Delta t \leq \frac{2}{\omega_{\max}}, \tag{15}$$

where $\omega_{\max}$ is the largest natural frequency of the system, rigorously obtained from the solution of the global eigenvalue problem

$$\det\left(\mathbf{H} - \omega^2 \mathbf{M}\right) = 0 \tag{16}$$

where, in the case of a linear system, $\mathbf{H}_0$ is a constant Hessian matrix. Proofs for this result, first stated in reference[16], can be found in reference[11] to reference[15].

Assembling of the global Hessian matrix is, however, a sheer contradiction with the spirit of DRM, one of the main advantages of it being the possibility of working only with global vectors.

Besides, definition of a global Δt may be quite non-economical, when the mesh is non-uniform, for instance when surfaces presents sharp variations in curvature, because it can be also shown that an upper limit approximation for the maximum frequency of the system is given by the *maximum maximorum* of the element frequencies, *i.e.*,

$$\omega_{\max} \leq \max_{e=1}^{n_e} \left\{ \omega_{e,\max} \right\} \tag{17}$$

where $\omega_{e,\max}$ is the maximum natural frequency of element e (see references[14,16]). Therefore, the smallest element determines the maximum allowable time-step.

Fortunately, Eq. (17) provides also a way to compute an upper bound for the time-step without the necessity of assembling the global stiffness matrix and –even more relevant– it also allows a *mass tuning procedure,* whereby the fictitious element nodal masses are adjusted in such a way that all the elements comply to a prescribed value Δt^* for the time increment, thus overcoming the limitations associated to non-uniform meshes.

A quite general and efficient mass tuning algorithm has been developed by the first author of this paper, a thoroughly discussion of which is deferred to a forthcoming paper.

3 FLEXIBLE BOUNDARIES

Area minimization with flexible boundaries requires the specification of an additional constrain, otherwise the problem becomes unbounded. Indeed, applying the so-called *soap film analogy*, which states that the area of membrane under a uniform isotropic stress field is minimal[1,2,3], it is perhaps easier to understand that it is impossible to have a minimal area with free boundaries, since stresses transversal to the membrane boundaries would be zero. Thus cables are always required, to equilibrate stresses along a membrane's boundary.

Here, however, we restrict the problem to purely geometric quantities, and an ingenious way to do so is to redefine the problem as a volume minimization, as done originally in

reference[9]. We thus add a thickness $h(\boldsymbol{x})$ to every point of the surface S, and we considered the surface to be bounded by flexible lines along its boundary ∂S, each of point of this lines endowed with an a cross-section area $A_\phi(\boldsymbol{x}_P)$. We also consider that the surface is restrained at some points $\boldsymbol{x}_{P_i}$, enough to avoid rigid body motions. The total volume of the system is given by

$$V = \int_S h(\boldsymbol{x})\, dA + \int_{\partial S} A_\phi(\boldsymbol{x})\, d\ell \,. \tag{18}$$

Now, analogously to (3), the necessary 1st order condition for a configuration $\boldsymbol{x}^*$ to present a minimum volume is given by the non-linear equation

$$\left.\frac{\partial V}{\partial \boldsymbol{x}}\right|_{\boldsymbol{x}^*} = 0\,, \tag{19}$$

with the equality restriction, $\left(\boldsymbol{x}_{P_i} - \bar{\boldsymbol{x}}_{P_i}\right) = \mathbf{0}, i = 1,\ldots,n_P$, where $\bar{\boldsymbol{x}}_{P_i}$ are prescribed coordinates at the n_P fixed points.

3.1 Face-volume elements

Assuming a *facet-volume* discretization for the surface, together with *line-volume* elements along its borders,

$$V \doteq \sum_{e=1}^{n_e} V^e \tag{20}$$

Also assuming a constant thickness inside a triangular facet, its unbalanced load vector is proportional to the quantity derived before, Eq. (9) . Thus, in this case,

$$\mathbf{p}^e = -\frac{h^e}{2}\boldsymbol{\Lambda}^e \mathbf{n}^e \tag{21}$$

3.2 Line-volume elements

We further assume that the surface boundary is divided into straight line segments connecting end nodes i and j and endowed with an uniform cross-section area A_ϕ^e, as shown in Figure 3. The current volume of such line-volume element is given by $V^e = A_\phi^e \ell^e$, where $\ell^e = \left\|\mathbf{x}_2^e - \mathbf{x}_1^e\right\|$ is the current element length.

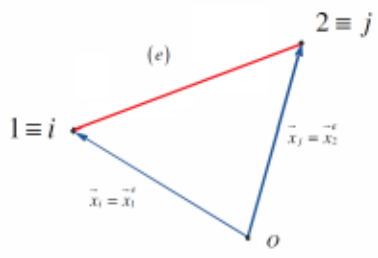

Figure 3: A line-volume element

The *line-volume element internal load vector* is thus given by

$$\mathbf{p}^e = \frac{\partial V^e}{\partial \mathbf{u}^e} = A_\phi^e \frac{\partial \ell^e}{\partial \mathbf{u}^e}. \tag{22}$$

After some algebra, we obtain

$$\mathbf{p}^e = A_\phi^e \begin{bmatrix} -\mathbf{v}^e \\ \mathbf{v}^e \end{bmatrix}, \tag{23}$$

where $\mathbf{v}^e = \left(\mathbf{x}_2^e - \mathbf{x}_1^e\right) / \left\|\mathbf{x}_2^e - \mathbf{x}_1^e\right\|$ is the unit vector connecting the end nodes of the line element. Once again, $\mathbf{p}^e$ is added to the global internal load vector according to (7), now with $\mathbf{C}_{1i}^e = \mathbf{C}_{2j}^e = \mathbf{I}_3$ and $\mathbf{C}_{1m}^e = \mathbf{C}_{2m}^e = \mathbf{0}$, $m \neq i, m \neq j$.

4 SOME BENCHMARKS

4.1 A Catenoid

Figure 4 shows a catenoid surface whose generatrix is given by $y(z) = a\cosh(z/a)$. The area of such surface is $A = 2\pi a\left(h + (a/2)\operatorname{senh}(2h/a)\right)$. We consider the catenoid delimited by two coaxial rings of radius 5.0m, distant 6.0m from each other, for which $h = 3.0\text{m}$, $a = 3.725355\text{m}$ and $A = 174.991064\text{m}^2$.

Table 1 shows the relative errors for three different approximations. In all cases, an initial cylindrical geometry connecting upper and lower rings was assumed, and a dynamic relaxation analysis was performed until the kinetic energy the model was damped out, which occurred after about 50 time-steps, for each model. We remark that faceting introduces an intrinsic error in area estimative, which is not related to the precision of the solution method.

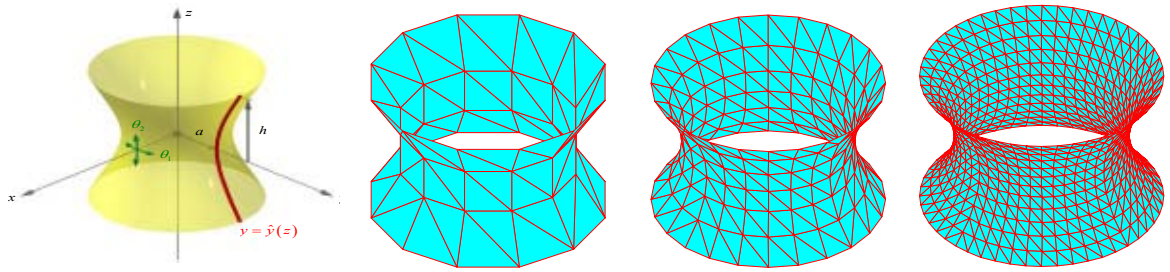

Figure 4: A catenoid surface and three different levels of discretization

Mesh	n_e	n_n	Area [m^2]	error
1	72	48	173.5658	8.5×10^{-3}
2	288	168	174.6246	2.1×10^{-3}
3	1152	624	174.9799	6.4×10^{-5}

Table 1: Area estimative for three different discretizations

4.2 A hyperbolic paraboloid with fixed borders

As a second benchmark we consider a hyperbolic paraboloid described by $z(x,y)=axy$, as depicted in Figure 5(a). Taking $a=0.1\text{m}$, $-5\text{m}\le x\le 5\text{m}$, $-5\text{m}\le y\le 5\text{m}$, the area of this surface can be calculated, to any required precision, by

$$A=\int_S\left(1+\left(\partial z/\partial x\right)^2+\left(\partial z/\partial y\right)^2\right)^{\frac{1}{2}}dA=\int_{-5}^{5}\int_{-5}^{5}\left(1+\left(0.1y\right)^2+\left(0.1x\right)^2\right)^{\frac{1}{2}}dx\,dy\approx 107.90370\text{m}^2.$$

A mesh with 1200 triangular facets and 645 nodes was adopted for the numerical solution. Figure 5(b) shows the initial mesh geometry, purposely far from the minimal configuration sought. Figure 5(c) shows the final configuration, with area A=107.9235m^2. About 200 time-steps were required to damp out the kinetic energy of the model.

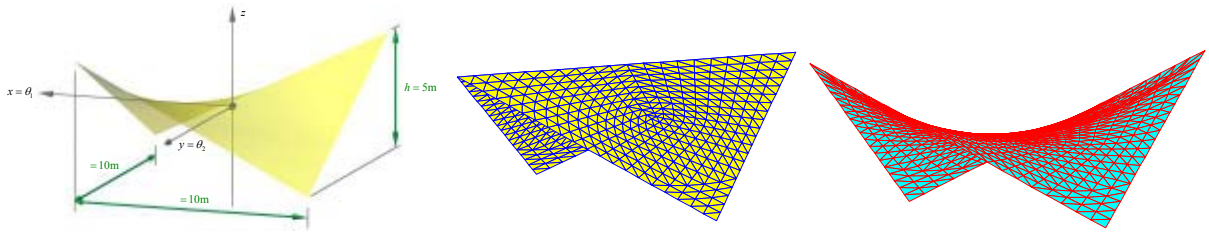

Figure 5: A hyperbolic paraboloid with fixed boundaries: (a) geometric parameters; (b) initial geometry; (c) final geometry.

4.3 A hyperbolic paraboloid with flexible borders

As a final example, we consider a hyperbolic paraboloid with flexible boundaries, taking the same mesh and initial geometry used in previous example. Only the displacements of the vertices are restrained, and a series of line-volume elements is arrange along the borders. Figure 6 shows the resulting geometries for $A_\phi=50$, $A_\phi=20$ and $A_\phi=10$, according to Eq. (22). About 250 time-steps are required to damp out the model's kinetic energy. Element distortion increases considerably as the borders' flexibility is increased, indicating that initial meshes laid onto geometries too far from solution may degrade considerably.

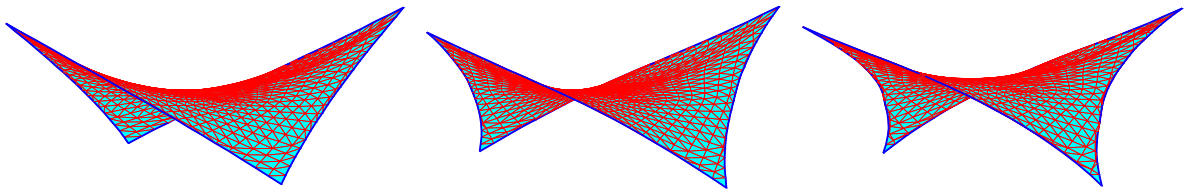

Figure 5: Some hyperbolic paraboloids with flexible boundaries:
(a) $A_\phi=50$; (b) $A_\phi=20$; (c) $A_\phi=10$.

4 CONCLUSIONS

- The Dynamic Relaxation Method (DRM) offers an interesting alternative to solve the area minimization problem, first interpreted as a nonlinear equilibrium problem, then replaced by a pseudo-dynamic analysis, where fictitious masses and damping matrices are arbitrarily chosen to control the stability of the time integration process;
- A discussion on the algorithms adopted for stability is postponed to a future paper, but we believe that the examples herein presented encourage the analyst to consider the application of DRM as a general method to solve nonlinear problems, not necessarily of mechanical nature.

REFERENCES

[1] Isenberg, C. *The Science of Soap Films and Soap Bubbles*, New York, USA, Dover Publications, 1992.

[2] Eisenhart, LP. *A Treatise on the Differential Geometry of Curves and Surfaces*, New York, USA, Dover Publications, 1960.

[3] Douglas, J. Solution of the Problem of Plateau, *Transactions of the American Mathematical Society*, No. **33**, 1, 1931, pp. 263-321.

[4] Gründig, L. Minimal Surfaces for Finding Forms of Structural Membranes, *Computers & Structures*, No. **30**, 3, 1988, pp. 679-683.

[5] Tabarrok, B., Qin, Z. "Nonlinear Analysis of Tension Structures", *Computers & Structures*, No. **45**, 5-6, 1992, pp. 973-984.

[6] Bletzinger, K-U., Wüchner, R., Daoud, F., Camprubí, N. Computational Methods for Form Finding and Optimization of Shells and Membranes, *Computer Methods in Applied Mechanics and Engineering*, No. **194**, 30-33, 2005, pp. 3438-3452.

[7] Souza, DCB., Pauletti, RMO., Almeida N., E. S. Sobre a Busca de Superfícies Minimais Aplicada às Tensoestruturas, *Congresso Ibero Latino-Americano sobre Métodos Computacionais em Engenharia*, Porto, 2007.

[8] Souza, DCB., Pauletti, RMO., Almeida Neto, ES. Finding minimal surfaces by direct area minimization, *IASS-SLTE International Symposium* 2008 - *New Materials and Technologies, New Design and Innovations A sustainable Approach to Architectural and Structural Design*, 2008, Acapulco.

[9] Arcaro, VF. and Klinka, KK. Finite element analysis for geometric shape minimization, Journal of the International Association for shell and Spatial Structures, **50,** 2, 79-88 (2009).

[10] Cundall, PA. *Explicit finite-difference methods in geomechanics*, Blacksburg, VA, (1976).

[11] Gondreau, GL. and Taylor, RL. Evaluation of Numerical Integration Methods in Elastodynamics, *Computer Methods in Applied Mechanics and Engineering*, 2, 69-97 (1972).

[12] Zienkiewicz, OC. and Taylor, RL. *The Finite Element Method*, 4th Ed. McGraw-Hill, London (1989).

[13] Hughes, TJR. *The Finite element Method – Linear Static and Dynamic Finite Element Analysis*, Prentice Hall Inc., Englewood Cliffs, N.J., 1987.

[14] Bathe, K-J, *Finite Element Procedures*, Prentice Hall, Prentice Hall Inc., Englewood Cliffs, N.J., 1996.

[15] Belytschko, T., Liu, WK., Moran, B. *Nonlinear Finite Elements for Continua and Structures*, John Wiley & Sons, NY, 2000.

[16] Irons, BM. and Treharne, C. A bound theorem for eigenvalues and its practical applications, *2nd Conf. on Matrix Methods in Structural Mechanics*, pp. 245-254, Wright-Patterson Air Force Base, Ohio, 9971.